A Demonstration of Magnetic Field Optimization in LHD

S. Murakami 1), H. Yamada 1), A. Wakasa 2), M. Sasao 1), M. Isobe 1), T. Ozaki 1), P. Goncharov 3), T. Saida 3), J. F. Lyon 4), M. Osakabe 1), K. Narihara 1), K. Tanaka 1), H. Inagaki 1), S. Morita 1), K. Ida 1), J. Miyazawa 1), H. Idei 1), K. Ikeda 1), S. Kubo 1), R. Kumazawa 1), T. Mutoh 1), Y. Oka 1), K. Saito 1), T. Seki 1), Y. Takeiri 1), Y. Torii 5), K. Tumori 1), T. Watari 1), K. Y. Watanabe 1), H. Funaba 1), M. Yokoyama 1), H. Maassberg 6), C. D. Beidler 6), K. Itoh 1), O. Kaneko 1), A. Komori 1), T. Akiyama1 7), N. Ashikawa 1), M. Emoto 1), M. Goto 1), K. Kawahata 1), H. Kawazome 8), K. Khlopenkov 1), T. Kobuchi 1), A. Kostrioukov 1), Y. Liang 1), S. Masuzaki 1), T. Minami 1), T. Morisaki 1), S. Muto 1), Y. Nagayama 1), Y. Nakamura 1), H. Nakanishi 1), Y. Narushima 1), K. Nishimura 1), N. Noda 1), T. Notake 1), H. Nozato 9), S. Ohdachi 1), N. Ohyabu 1), B. J. Peterson 1), A. Sagara 1), S. Sakakibara 1), R. Sakamoto 1), K. Sato 1), M. Sato 1), T. Shimozuma 1), M. Shoji 1), H. Suzuki 1), N. Takeuchi 5), N. Tamura 1), K. Toi 1), T. Tokuzawa 1), Y. Xu 1), I. Yamada 1), S. Yamamoto 5), T. Yamamoto 5), Y. Yoshimura 1), M. Yoshinuma 1), M.Y. Tanaka 1), S. Okamura 1), S. Yoshimura 1), K. Nagaoka 1), T. Satow 1), S. Imagawa 1), T. Mito 1), I. Ohtake 1), T. Uda 1), K. Ohkubo 1), S. Sudo 1), K. Yamazaki 1), K. Matsuoka 1), O. Motojima 1), Y. Hamada 1), M. Fujiwara 1)

1) National Institute for Fusion Science, Toki, Gifu 509-5292, Japan
2) Graduate School of Engineering, Hokkaido University, Sapporo 060-8628, Japan
3) Department of Fusion Science, School of Mathematical and Physical Science, Graduate University for Advanced Studies, Hayama, 240-0193, Japan
4) Oak Ridge National Laboratory, Oak Ridge, TN 37831-8072, USA
5) Department of Energy Engineering and Science, Nagoya University, 464-8603, Japan
6) Max-Planck-Institut fuer Plasmaphysik, EURATOM Ass., D-17491 Greifswald, Germany
7) Research Laboratory for Nuclear Reactors, Tokyo Institute of Technology, Tokyo 152-8550, Japan
8) Graduate School of Energy Science, Kyoto University, Uji 611-0011, Japan
9) Graduate School of Frontier Sciences, The University of Tokyo 113-0033, Japan

e-mail contact of main author: murakami@nifs.ac.jp

Abstract. An optimized configuration of the neoclassical transport and the energetic particle confinement to a level typical of so-called “advanced stellarators” is found by shifting the magnetic axis position in LHD. Electron heat transport and NBI beam ion distribution are investigated in low-collisionality LHD plasma in order to study the magnetic field optimization effect on the thermal plasma transport and the energetic particle confinement. A higher electron temperature is obtained in the optimized configuration, and the transport analysis suggests a considerable effect of neoclassical transport on the electron heat transport assuming the *ion-root* level of radial electric field. Also a higher energetic ion distribution of NBI beam ions is observed showing the improvement of the energetic particle confinement. These obtained results support a future reactor design by magnetic field optimization in a non-axisymmetric configuration.

1. Introduction

Improvement of the energetic particle confinement and the reduction of the neoclassical transport are key issues in the development of a reactor based on the helical system. Recently, efforts have been undertaken to find configurations having both significantly reduced neoclassical transport and good MHD stability, so-called ``advanced stellarators''. However, the effects of magnetic optimization on the thermal transport and the energetic particle confinement have not been experimentally verified satisfactorily. The experimental

demonstration of the magnetic field optimization (``advanced stellarators'' level) is required for the prospect of a reactor design based on the magnetic field optimization.

On the other hand, the Large Helical Device (LHD)[1] has been constructed as a standard heliotron type device, where a configuration called the ``standard'' configuration, with the magnetic axis at a major radius of R_{ax}=3.75m, has been proposed. This configuration satisfies the requirements for good plasma performance, i.e. good particle confinement, high plasma beta, and the presence of a divertor. However, a relatively large effective helical ripple exists and the existence of strong positive radial electric field (*electron-root*) is indispensable for the reactor design in this configuration. To exclude this condition, further optimization of neoclassical transport is possible[2,3] if we exclude the ideal MHD stability condition[4].

LHD experiments started in 1998 and have shown good plasma[5-7]. The experiments have been performed not only in the standard configuration (R_{ax}=3.75m) but also in the ``inward shifted'' configuration (R_{ax}=3.6m), in which the ideal MHD stability analysis predicts instability. Interestingly, however, no degradation of the plasma confinement has been observed in the experimental plasma of the R_{ax}=3.6m configuration and, furthermore, the energy confinement is found to be better than that of the R_{ax}=3.75m case[8]. The similar improvement of plasma confinement in the inward shifted configuration was also observed in the CHS[9]. These facts suggest that the MHD stability problem is not a severe one for plasma confinement in heliotron and makes it reasonable to consider shifting the magnetic axis further inwards where further improvement of the neoclassical transport can be expected in LHD. Actually, LHD can be operated in the configuration shifting the magnetic axis from 3.45m to 4.05m.

In this paper, we show an optimized configuration in LHD to a level typical of so-called “advanced stellarators”, and demonstrate experimentally the effect of magnetic field optimization on the thermal plasma transport and the energetic particle confinement.

2. Magnetic field optimization in LHD

The shift of the magnetic axis alters the magnetic field configuration in flux coordinates. In the R_{ax}=3.75m (``standard'' configuration) case there are two dominant magnetic field components, the main helical curvature term, $B_{2,10}$, and the toroidal curvature term, $B_{1,0}$, and an additional small component $B_{1,10}$. Shifting the magnetic axis inwards to R_{ax}=3.6m, two side bands of the main helical curvature term, $B_{1,10}$ and $B_{3,10}$, increase and their amplitudes become comparable to that of $B_{1,0}$. Then the R_{ax}=3.6m configuration conforms to a ``□-optimized'' field[10], where the neoclassical transport would be significantly improved relative to a standard heliotron configuration. A further inward shift of the magnetic axis increases the toroidal mirror term, $B_{0,10}$, in addition to the two side band terms.

We evaluate a mono-energetic local transport coefficient using DCOM (Diffusion COefficien calculator by Monte-Carlo method)[11,12] in which test particle orbits are followed solving the equations of motion in Boozer coordinates and the transport coefficient is evaluated statistically from the mean square displacement of the particles. Thus, DCOM can be applicable to the local neoclassical transport analysis and the global simulation code, e.g. GNET[13], should be applied in the case where the large orbit size of trapped particle plays an important role.

The diffusion coefficients are evaluated for configurations with different magnetic axis

positions, R_{ax}, at three different normalized plasma radii; r/a =0.25, 0.5, and 0.75. In this study we assume electrons as test particles with an energy of 3keV. The magnetic field is set to 3T at the magnetic axis. We select two typical collision frequencies, ν; one is ν=3.16 x 10^3 sec^{-1}, at which a 3keV electron is in the $1/\nu$ regime and the other is ν=3.16 x 10^5 sec^{-1}, at which the electron is in the plateau regime. Figure 1 shows the normalized mono-energetic transport coefficients, $D^*(=D/D_p)$, in the $1/\nu$ and the plateau regimes. The transport coefficients are normalized by the plateau value of the equivalent circular tokamak, $D_p=(\pi/16)(v^3/\iota R\omega_c^2)$, where v, R, ι and ω_c are the electron velocity, the major radius, the rotational transform, and the cyclotron frequency, respectively.

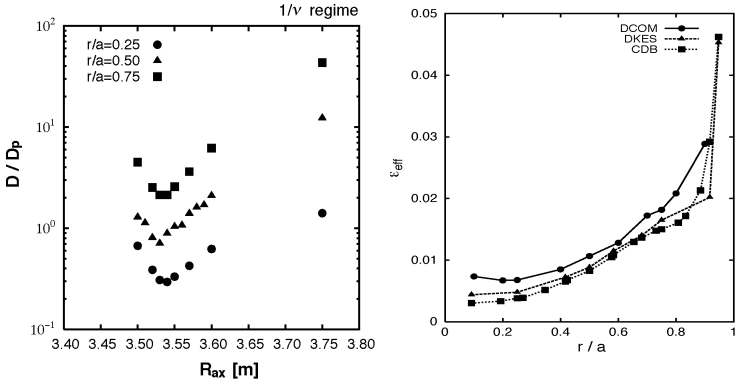

FIG. 1. Plots of the normalized neoclassical transport coefficients evaluated by DCOM in the $1/\nu$ regime (left) and the radial profiles of the effective helical ripple in the R_{ax}=3.53m configuration evaluated by DCOM, DKES, and an analytic formula (right).

We can see a strong reduction of the diffusion coefficient by shifting the magnetic axis inwards from R_{ax}=3.75m and an optimum point is found around R_{ax}=3.53m in the $1/\nu$ regime in Fig. 1 (top). Interestingly, the radial dependence of the optimum axis position is weak and the optimum positions are at R_{ax}=3.53m in the r/a=0.5 and 0.75 cases, and at R_{ax}=3.54m in the r/a=0.25 case. Thus, although a bit arbitrary, we shall define the R_{ax}=3.53m configuration as the neoclassical-transport-optimized configuration of the LHD.

In the plateau regime the diffusion coefficient decreases monotonically by shifting the magnetic axis inwards. This is due to the reduction of $B_{1,0}$, and also the coupling of the toroidal and helical contributions by $B_{1,10}$[11]. A similar coupling of the toroidal and helical contributions in the plateau regime is also found in helias configuration[14].

In order to compare the neoclassical transport level with that of other devices, the effective helical ripple for $1/\nu$ transport, ε_{eff}, is evaluated by the relation between the transport coefficients and collision frequency in the $1/\nu$ regime. Figure 1(rihght) shows the radial profile of ε_{eff} in the R_{ax}=3.53m configuration evaluated by DCOM, DKES[15,16] and a recently developed analytic formula by C.D. Beidler, et. al[17]. All three results show a very small value of ε_{eff} with the values obtained less than 1% up to r/a=0.5 and less than 2% up to r/a=0.8. Beyond r/a=0.8, ε_{eff} increases rapidly up to 5 %.

Next we study the energetic ion confinements in strongly inward shifted configurations of LHD. Collisionless α particle confinements are investigated assuming reactor sized devices (α particle; 3.4MeV, Plasma volume; 1000 m^3, and Magnetic field; 5 T)[18] based on three typical configurations of LHD with different magnetic axis positions in the major radius; R_{ax}=3.75m, 3.6m, 3.53m.

Figure 2 shows typical orbits of helically trapped α particles in the three configurations of reactor sized LHD; R_{ax}=3.75m (left) and 3.53m (right). We plot the toroidal projection of the

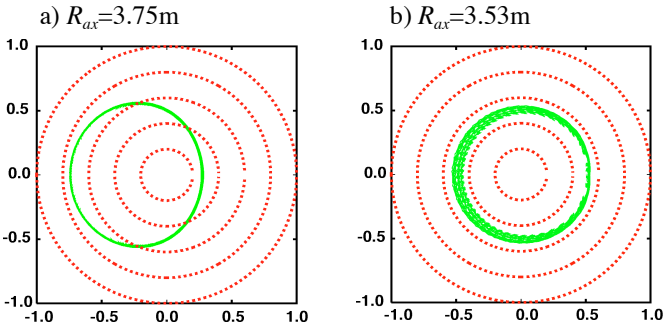

FIG. 2. Typical orbit of a helically trapped particle (pitch angle: 0.47□) in the three configurations of reactor sized LHD based on the R_{ax}=3.75m (left) and 3.53m d (right) configurations.

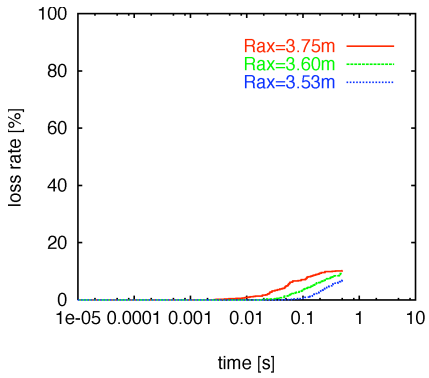

FIG. 3. Time development of alpha-particle loss rates in the three configurations of reactor sized LHD.

orbits in the Boozer coordinates. The co-centric circles correspond to magnetic surfaces. We can see the deviation of the trapped particle orbit from the magnetic surfaces reduced by shifting the magnetic axis position inwardly. The deviation almost disappears in the R_{ax}=3.53m case.

We evaluate the loss rate of □□particles as a function of time in Fig. 3. It is found that there is no loss before 0.01 s but the loss rate increases after 0.01s in the R_{ax}=3.75m case. However the loss of □□particle starts after the energy slowing down time (~0.1s) in the R_{ax}=3.53m case. Thus a sufficient confinement of □□particle is obtained in the R_{ax}=3.53m configuration for a helical reactor.

Consequently, the neoclassical transport analysis shows the optimum configuration with respect to 1/□ transport. Also the deviation of trapped particle orbit from magnetic surfaces is very small and good confinement of □□particle is obtained for a time longer than the energy slowing-down time in the reactor scaled device. These facts indicate flexibility of LHD configuration from the standard helical to an optimized configuration with a level typical of so-called``advanced stellarators'' (a small effective helical ripple < 2% and a good energetic particle confinement during the energy slowing-down time).

3. Optimization effect on thermal plasma transport

The electron heat transport in the long-mean-free-path regime (1/□ regime) is investigated to clarify the magnetic field optimization effect on the thermal plasma transport in the LHD. The electron heat transport coefficients are estimated by shifting the magnetic axis position, R_{ax}. We considered three typical configurations; R_{ax}=3.45m, 3.53m and 3.6m. In order to compare the electron heat transport we set the magnetic field strength so that the heating deposition profile is similar in the three configurations. Because we cannot set the ECH resonance point to the magnetic axis in the R_{ax} = 3.6m case, the heating deposition is adjusted to distribute inside of $r/a < 0.2$.

Figure 4 shows a comparison of electron temperatures obtained by the Thomson scattering system (center) in the three configurations (R_{ax} = 3.45m [#32347, t=0.42s], 3.53 m [#32303, t=0.52s] and 3.6 m [#32123, t=0.52s]) with nearly the same density profile (left). The fitted curves of the electron temperatures are also shown in the Fig. 3 (right). We cannot see a clear difference in the electron temperature in the region $r/a > 0.7$, though a higher electron

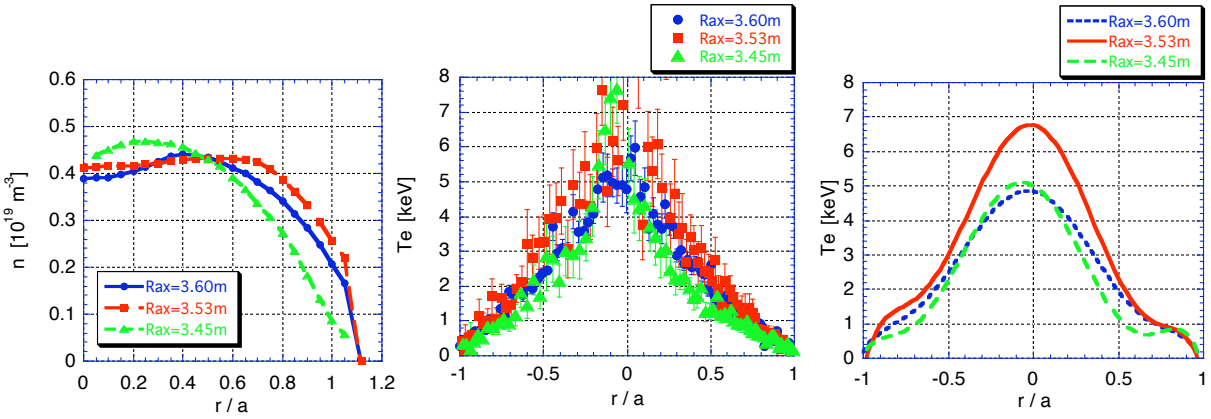

FIG. 4. Comparisons of the radial profiles of the density (left), the electron temperature (center), and the fitted curves of the electron temperatures (right) in the three configurations (R_{ax} = 3.45m [#32347, t=0.42s], 3.53 m [#32303, t=0.52s] and 3.6 m [#32123, t=0.52s]).

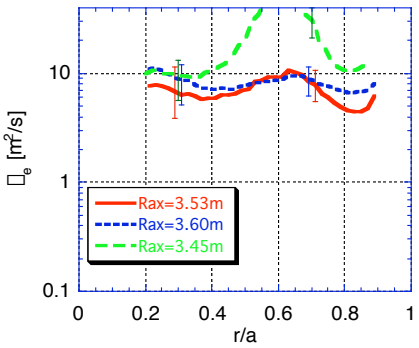

FIG. 5. The estimated effective electron heat transport coefficients in the three configurations.

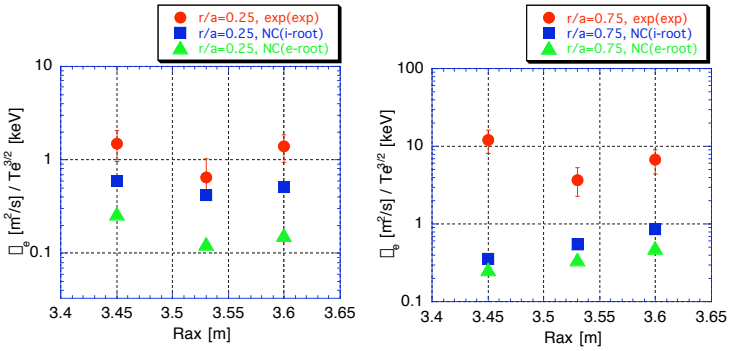

FIG. 6. Comparisons of the neoclassical transport and the experimentally observed electron heat transport at r/a=0.25 (left) and 0.75 (right).

temperature is observed in the central region ($r/a < 0.4$) in the R_{ax} = 3.53 m configuration case. Near the magnetic axis the electron temperature rapidly increases in the R_{ax} = 3.45 m case. This would be due to the rather peaked ECH deposition profile compared with other two configurations.

The estimated effective electron heat transport coefficients, χ_e, are plotted in Fig. 5. The obtained χ_e shows nearly the same value around 10m^2/s from r/a=0.2 to 0.4 even though the different electron temperatures in three configuration cases. Considering a strong electron temperature dependency of χ_e, this indicates an improvement of χ_e in the central region ($r/a <$ 0.4) in the R_{ax}= 3.53m case, where the highest electron temperature is observed. We can see the increase of χ_e near r/a=0.6 in the R_{ax}= 3.45m case is due to the temperature flattening from r/a=0.5 to 0.7.

We analyze the neoclassical transport using the DCOM code to show the role of neoclassical transport. In this experiment there is no measurement of the radial electric field, E_r, and ion temperature profile. So as a first step we evaluated the neoclassical transport coefficient assuming E_r values of the *ion-root* (~1kV) and *electron-root* (~6kV) levels. Figure 6 shows the comparisons of the neoclassical transport and the experimentally observed electron heat

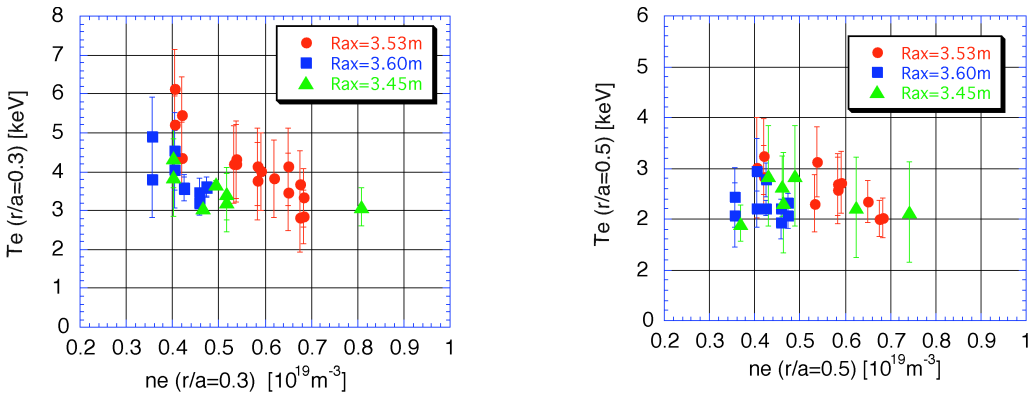

FIG. 7. Comparisons of the density dependencies of the electron temperature in the three configurations at r/a=0.3 and 0.5.

transport at r/a=0.25 (left) and 0.75 (right). We can see the considerable effect of neoclassical transport if we assume the *ion-root* level of E_r at r/a=0.25, while the neoclassical transport coefficient becomes several times smaller than the experimental ones if we assume the *electron-root* level of E_r. At r/a=0.75 the neoclassical transport is one order of magnitude smaller than experimental values in both E_r cases.

In the LHD the *ion-root* level of E_r is usually observed except in the case with the ITB-like steep electron temperature gradient. Thus we consider that the *ion-root* level of E_r is plausible and the improvement of electron heat transport would be due to the neoclassical transport optimization. Even in the *electron-root* case, we can emphasize that the anomalous transport in addition to neoclassical transport is reduced in the neoclassical-transport-optimized configuration of the LHD. The radial electric field will be measured and its effects will be clarified in the near future.

Figure 7 shows the comparison of the density dependence of the electron temperature in the three configurations at r/a=0.3 and 0.5. We found that the achieved electron temperature at r/a =0.3 is higher in the R_{ax} = 3.53m case compared with two other configurations and this difference shrinks as the density increases. At r/a =0.5 the difference becomes smaller and no clear difference can be seen among the three configurations.

4. Optimization effect on energetic particle confinement

The NBI beam ion distribution is investigated to clarify the magnetic field optimization effect on the energetic particle confinement in the LHD. The count rates of the neutral particle analyzers are compared during NBI heating by shifting the magnetic axis position, R_{ax}. We considered three typical configurations with R_a values near optimized point (3.53m, 3.6m and 3.75m). Figure 8 shows the energy loss rate by orbit loss evaluated by GNET[13] as a function of R_{ax}. In the LHD the tangential injection NBI heating is applied and the fraction of energy loss by orbit loss is normally small. So, this predicts a significant improvement of trapped energetic particle confinement in inward shifted configuration.

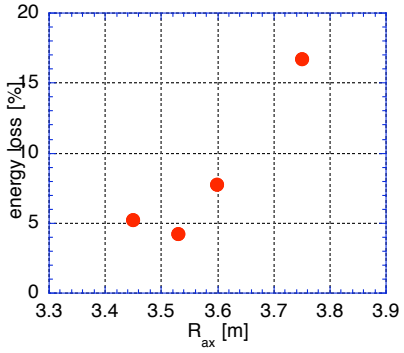

FIG.8. R_{ax} dependency of NBI heating energy loss rate by orbit loss evaluated by GNET

We study the NBI beam ion distribution by silicon detector-based neutral particle analyzer (SDNPA). A compact quasilinear horizontal array of six ion-implanted silicon detectors is used and a vertically movable collimating aperture provide two-dimensional scan of the non-axisymmetric LHD plasma column. The angle between the sight lines in the horizontal direction is 4.6 degrees. The angular sector observable due to the vertical scan is 14 degrees. The geometry of experiments is shown in Fig. 9. We evaluate the neutral particle count in the pitch angle region of trapped and partially trapped particles and compared the results changing the magnetic axis position with nearly same density (~0.7x$10^{19}$$m^{-3}$) and heating power

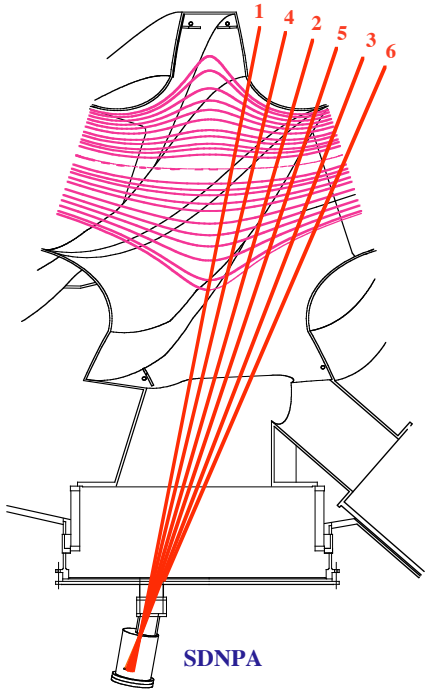

FIG. 9. SDNPA viewing chords

Figure 10 shows the comparisons of the normalized count rate of the three configurations for the chord #6 (left) and #2 (right). SDNPA chord #6 measures the pitch angle of 40 to 50 degrees and #2 is from 55 to 65 degrees. The initial pitch angles of NBI beam ions are less than 45 degrees. Because the thermal plasma confinement depends on R_{ax} in LHD, the obtained electron temperature is higher in the inward shifted case. So we normalized the count rate by the count rate at the slightly lower energy of the beam injection (140keV) so that we can directly compare the slowing-down process excluding the count rate difference due to the difference of the slowing-down time.

We can see the difference of the slope from injection energy to the thermal energy in the chord #6 (Fig. 10, left). In the R_{ax}=3.53m case larger increase of the normalized count number can be seen compare with others. The count rate is decreased until around 100keV in the R_{ax}=3.75m case. In this energy region the energy slow-down by electron plays dominant role in beam ion collisions with thermal plasma and this difference due to the radial diffusion of transition particle. We also can see the higher count rate in the R_{ax}=3.53m case in the chord #2 (Fig. 10, right).

To see more clearly the difference of count rate in the chord #6. We plot the ratio of the count rate between at the energy of 140keV and 100keV as a function of slowing down time in the

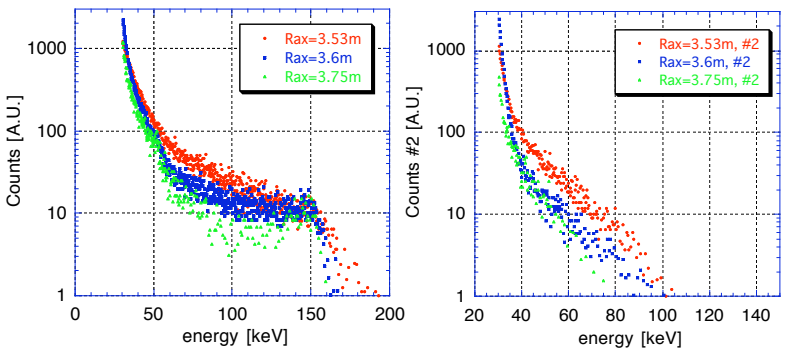

FIG. 10. Comparisons of normalized counts rate by SDNPA with the similar density in the three configuration of LHD.

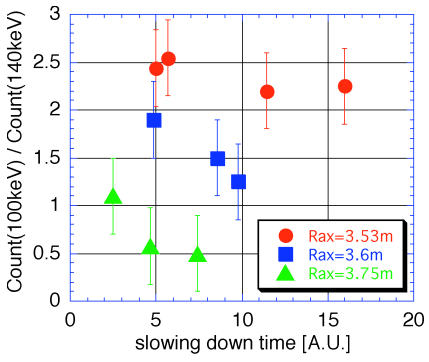

FIG. 11. Plot the ratio of the count rate between at the energy of 140keV and 100keV as a function of slowing down time.

three configurations. A clear difference can be seen in the three configurations. We can see the higher ratio in the R_{ax}=3.53m case compared with other two cases. In these cases the ratio goes up as the slowing-down time become short, because the effect of radial diffusion get smaller in the shorter slowing-down time case.

5. Conclusion

We have, first, studied the neoclassical transport for LHD configurations in which the magnetic axis has been shifted radially. With respect to 1/ transport, the optimum configuration is found when the magnetic axis has a major radius of 3.53m. Also, in this configuration, the deviation of trapped particle orbit from magnetic surfaced is very small and a good confinement of particle is obtained for a time longer than the energy slow-down time in the reactor scaled device. These facts indicate that a strong inward shift of the magnetic axis can optimize the LHD configuration to a level typical of so-called``advanced stella-rators'' (a small effective helical ripple < 2% and a good energetic particle confinement during the energy slowing-down time).

Then, we experimentally demonstrate the effect of magnetic optimization on the thermal plasma transport and the energetic particle confinement in LHD. The experimental results in low collisionality plasmas show a higher electron temperature and a higher trapped ion distribution in the optimized configuration. These obtained results show further possibility of a heliotron type configuration and support a future reactor design by magnetic field optimization in a non-axisymmetric configuration.

References

[1] IIYOSHI, A., et al., Nucl. Fusion **39** (1999) 1245.
[2] TODOROKI, J., J. Phys. Soc. Jpn. **59** (1990) 2758.
[3] MURAKAMI, S., Nucl. Fusion **39** (1999) 1165.
[4] ICHIGUCHI, K., et al., Nucl. Fusion **33** (1993) 481.
[5] FUJIWARA, M., et al., Nucl. Fusion **39** (1999) 1659.
[6] MOTOJIMA, O, et al.,Phys. Plasmas **6** (1999) 1843.
[7] FUJIWARA, M, et al., Nucl. Fusion **40** (2000) 1157
[8] YAMADA, H., et al., Plasma Phys. Control. Fusion, **43**, A55(2001).
[9] OKAMURA, S., et al., Nucl. Fusion **39**, 1337(1999).
[10] MYNICK, H.E., CHU, T.K., and BOOZER, A.H., Phys. Rev. Lett. **48** (1982) 322.
[11] WAKASA, A., et al., J. Plasma Fusion Res. SERIES, Vol. **4**, 408(2001).
[12] MURAKAMI, S., et al., Nucl. Fusion **42** (2002) L19.
[13] MURAKAMI, S., et al., Nucl. Fusion **40** (2000) 693.
[14] BEIDLER, C.D. and MAASSBERG, H., in Theory of Fusion Plasmas (Proc. Joint Varenna-Lausanne International Workshop, Varenna, 1996), Editrice Compositori, Bologna (1996) 375.
[15] HIRSHMAN, S.P., et al., Phys. Fluids **29** (1986) 2951.
[16] MAASSBERG, H., et al., Phys. Fluids B **5** (1933) 3627.
[17] BEIDLER, C.D. and MAASSBERG, H., Plasma Phys. Control. Fusion **43** (2001) 1131.
[18] MURAKAMI, S., et al., J. Plasma Fusion Res. SERIES, Vol. 5 (in press).
[19] LYON, J.F., SPONG, D.A, J. Plasma Fusion Res. SERIES, 1, 358 (1998)
[20] GONCHAROV, P.R., et al. J. Plasma Fusion Res. SERIES, 5 (in press)
[21] LYON, J.F., et al. Proc. 14th High-Temp. Plasma Diagn. Conf., Rev. Sci. Instr. (to be published).